communications chemistry

A Nature Portfolio journal

Article

https://doi.org/10.1038/s42004-025-01829-z

A theoretical study on the feasibility of 1,4-Copper migration in the Cu-catalyzed formal hydro(borylmethylsilyl)ation of internal alkynes

Check for updates

Song Liu [1,2] ✉, Wei Chen [1] ✉, Xinyu Long[3], Dianmin Zhang[1], Jingxu Chen[1], Zhou Zhu[1] & Haobin Wei[1]

The 1,n-metal migration process is distinct from traditional bond-forming pathways and offers a unique approach for constructing complex organic architectures. However, in contrast to the well-documented Pd-, Rh-, Fe-, Co-, and Ni-catalyzed migration coupling reactions, studies on Cu-catalyzed variants are scarce. This report describes density functional theory (DFT) calculations aiming to investigate the mechanism of Cu-catalyzed formal hydro(borylmethylsilyl)ation, which is proposed to occur via 1,4-copper migration. The computational results support a metal non-migration mechanism. The stereoselectivity of the reaction is determined by the energy difference between the proton transfer transition state and the anionic releasing transition state after syn-to-anti isomerization. Additionally, DFT calculations were used to evaluate the effects of various substituents on the internal alkyne. Overall, this study offers a solid theoretical basis for experimental investigations into Cu-catalyzed migration coupling reactions.

Recent studies have investigated the migratory behavior of transition metals in catalytic coupling reactions, with increasing emphasis on optimizing catalytic efficiency through the precise modulation of metal migration dynamics[1–5]. The 1,n-metal migration process, whereby a transition metal relocates between carbon atoms during catalysis, offers a unique strategy for assembling complex organic architectures that does not involve classical bond-forming pathways. Indeed, Pd[6–10]- and Rh[11–14]-mediated 1,n-migrations have been systematically explored, and notably, recent studies have demonstrated the potential of earth-abundant 3 d transition metals (e.g., Fe[15,16], Co[17–22], Ni[23–30]) as migratory centers, thus offering cost-effective alternatives to precious metal catalysts. Nevertheless, compared with the established Fe-, Co-, and Ni-catalyzed migration coupling reactions, reports on Cu-catalyzed reactions are rare[31] (Scheme 1a).

Recently, Shintani et al. reported the copper-catalyzed regio- and stereoselective formal hydro(borylmethylsilyl)ation of internal alkynes, which involved 1,4-copper migration from an alkenyl carbon to an alkyl carbon[31] (Scheme 1b). Under optimal conditions, the alkenylsilylmethylboronate product **3a** was isolated in 65% yield, with the stereoselectivity for **3a** over **4a** being 94:6. Kinetic studies, NMR analyses, and deuterium-labeling experiments were consistent with a 1,4-copper migration process. However, the precise mechanism of this migration remains unclear, and there are lingering uncertainties regarding whether this migration process actually occurred.

Metal migration mechanisms can be classified into three main categories. (i) Oxidative addition of a metal (M) into a C–H bond can result in new C–M and M–H bonds, which undergo reductive elimination, thereby facilitating metal migration by cleaving the original C–M bond [3b [32,33]]. (ii) Activation of C–H bonds in the presence of a base can generate C–M bonds via a cooperative metalation-deprotonation (CMD) mechanism. After subsequent protonation, this process allows for metal migration through various combinations[34,35]. (iii) β-H elimination can form metal-hydride species and alkenes, which can reinsert into the M–H bond via metal migration. A sequence of β-H eliminations followed by reinsertions can facilitate multiple metal migration steps[36–38].

In the hydro(borylmethylsilyl)ation reaction shown in Scheme 1b, the alkenyl-Cu(I) intermediate **I** can follow one of three migration pathways to undergo 1,4-copper migration. However, the d-electron configuration of Cu(I) and the inherent instability of a Cu(III) intermediate typically lead to a

[1]Chongqing Key Laboratory for Resource Utilization of Heavy Metal Wastewater, College of Chemistry and Environmental Engineering, Chongqing University of Arts and Sciences, Yongchuan, 402160, PR China. [2]School of Chemistry and Chemical Engineering, Chongqing University, Chongqing, 400030, China. [3]Chongqing Key Laboratory of Materials Surface & Interface Science School of Materials Science and Engineering, Chongqing University of Arts and Sciences, Yongchuan, 402160, China. ✉e-mail: sliu@cqwu.edu.cn; envwchen@163.com

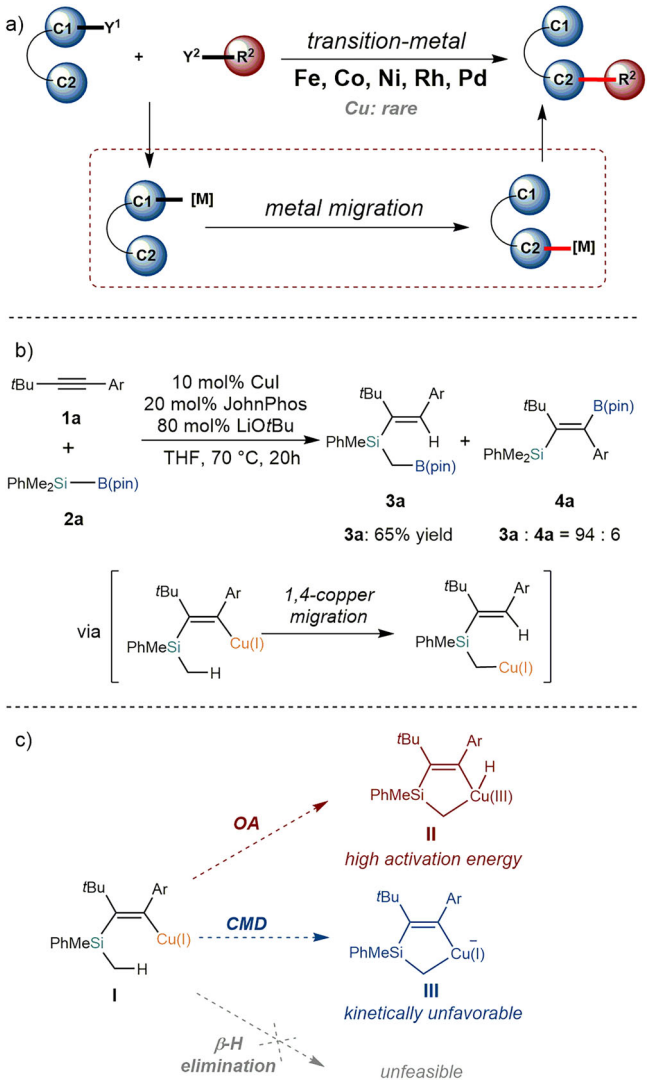

Scheme 1 | The state of the art in transition-metal-catalyzed migration coupling reactions. **a** Transition-metal-catalyzed coupling reactions that involve 1,n-metal migration. **b** Cu-catalyzed formal hydro(borylmethylsilyl)ation of an internal alkyne. **c** Proposed 1,4-copper migration mechanistic pathways.

high activation energy for the oxidative addition (OA) of the Cu(I) center into the C(sp^3)–H bond[39–41] (Scheme 1c). Additionally, although the CMD mechanism is commonly observed with Cu(II), this process is kinetically unfavorable for Cu(I)[42–45]. Finally, the structural constraints of this intermediate hinder the *β*-H elimination mechanism. Thus, the potential 1,4-copper migration process in this reaction requires further elucidation through detailed computational studies.

This report presents a theoretical investigation of the mechanism and origin of stereoselectivity of this Cu-catalyzed formal hydro(borylmethylsilyl)ation reaction. The results offer a plausible detailed reaction mechanism and reactivity profile. Computational findings indicate that the 1,4-copper migration pathway is kinetically unfavorable. The alkenyl-Cu(I) intermediate, which is formed via alkyne migration insertion, undergoes anion exchange, proton transfer, and nucleophilic substitution to yield the alkenylsilylmethylboronate product[46–51]. The results presented herein provide a theoretical framework for guiding further experimental investigations of Cu-catalyzed coupling reactions.

Computational methods

All density functional theory (DFT) calculations were conducted using the GAUSSIAN 16[52] software suite. The B3-LYP-D3[53–58] density functional was employed for geometric optimization, utilizing a standard 6-31 G(d) basis set. The SDD basis set was specifically applied for copper. Harmonic frequency calculations were conducted for all stationary points to confirm their classification as local minima or transition state structures and to obtain thermochemical corrections for enthalpies and free energies. All local minima exhibited zero imaginary frequencies, while each transition state presented a single imaginary frequency. Solvent effects were included by performing single-point calculations on gas-phase stationary points using the SMD[59] continuum solvation model. The M11-L[60] functional was employed alongside the def2-TZVP[61,62] basis set to calculate single-point energies in tetrahydrofuran solvent. The optimized structures were visualized using CYLview[63]. The independent gradient model (IGM)[64] was applied utilizing the M11-L DFT method with the def2-TZVP basis set, employing the Multiwfn[65] and VMD[66] programs. The oxidation state calculations were also conducted using the Multiwfn program. To accurately evaluate the entropy of the dual metal catalysis pathway, the solution-translational entropy correction was recalculated using the THERMO[67] program.

Results and discussion

Based on reported experimental results and control experiments, we proposed the reaction mechanisms illustrated in Scheme 2. Scheme 2a depicts potential mechanisms for 1,4-copper migration, and Scheme 2b presents the potential mechanisms for metal non-migration. The results from 1H NMR spectroscopy indicated that the anionic bis(phenyldimethylsilyl)cuprate **A** was generated in situ from a 1:2 mixture of CuI and silylboronate **2a** in the presence of LiOtBu (4.0 equiv)[31]. Notably, when *tert*-butyl(phenyl)acetylene **1a** was added to the in-situ generated Cu($SiMe_2Ph$), no reaction occurred. Conversely, a smooth reaction was observed at room temperature when **1a** was added to the in-situ generated **A**, resulting in the formation of silylalkenyl(silyl)cuprate (see Supporting Information)[31]. Consequently, we selected the anionic bis(phenyldimethylsilyl)cuprate **A** as the catalytically active species in this hydro(borylmethylsilyl)ation reaction. The internal alkyne substrate **1a** inserts into the Cu(I)–Si bond, thereby forming the silane-substituted alkenyl-Cu(I) anion intermediate **B**. In Path I, the C(sp^3)–H bond undergoes oxidative addition with the Cu(I) center, generating the alkenyl- and alkyl-Cu(III) intermediate **C**. Intermediate **C** then undergoes reductive elimination, yielding the alkyl-Cu(I) intermediate **D**, thus completing the 1,4-copper migration. The subsequent metathesis between intermediate **D** and silylboronate **2a** affords the alkenylsilylmethylboronate product **3a** and regenerates the catalytically active species **A**, which completes the catalytic cycle. In Path II, the alkenyl-Cu(I) anion intermediate **B** can also participate in a CMD process, using a *tert*-butoxide ion as a base to form the alkenyl- and alkyl-Cu(I) intermediate **E**. Subsequent protonation of the allyl C–Cu(I) bond yields the alkyl-Cu(I) intermediate **D**.

As shown in Scheme 2b, anion exchange between the silicon anion and the alkenyl-Cu(I) anion intermediate **B** results in the formation of the alkenyl-carbanion intermediate **F** and the regeneration of the catalytically active species **A**. In Path III, subsequent proton transfer from the methyl group to the alkenyl moiety generates the alkyl carbanion intermediate **G**. This intermediate then undergoes a nucleophilic substitution with silylboronate **2a**, yielding the alkenylsilylmethylboronate product **3a**. Alternatively, in Path IV, the syn-to-anti isomerization of the alkyl carbanion **F** generates the anti-alkyl carbanion intermediate **H**. A nucleophilic substitution reaction between intermediate **H** and silylboronate **2a** then produces the silylalkenylboronate by-product **4a**.

The free energy profiles associated with the formation of the anionic bis(phenyldimethylsilyl)cuprate active catalyst are shown in Fig. 1. The nucleophilic addition of the *tert*-butoxide anion into the silylboronate substrate **2a** occurs via transition state **TS1**, which has an energy barrier of 11.3 kcal/mol and leads to the anionic boron intermediate **INT1**. In **TS1**, the O–B bond length is 2.81 Å. Release of the anionic silicon intermediate **INT2** from **INT1** occurs through transition state **TS2**. The free energy of **INT2** is −24.2 kcal/mol, indicating that **INT2** is predominant in the reaction

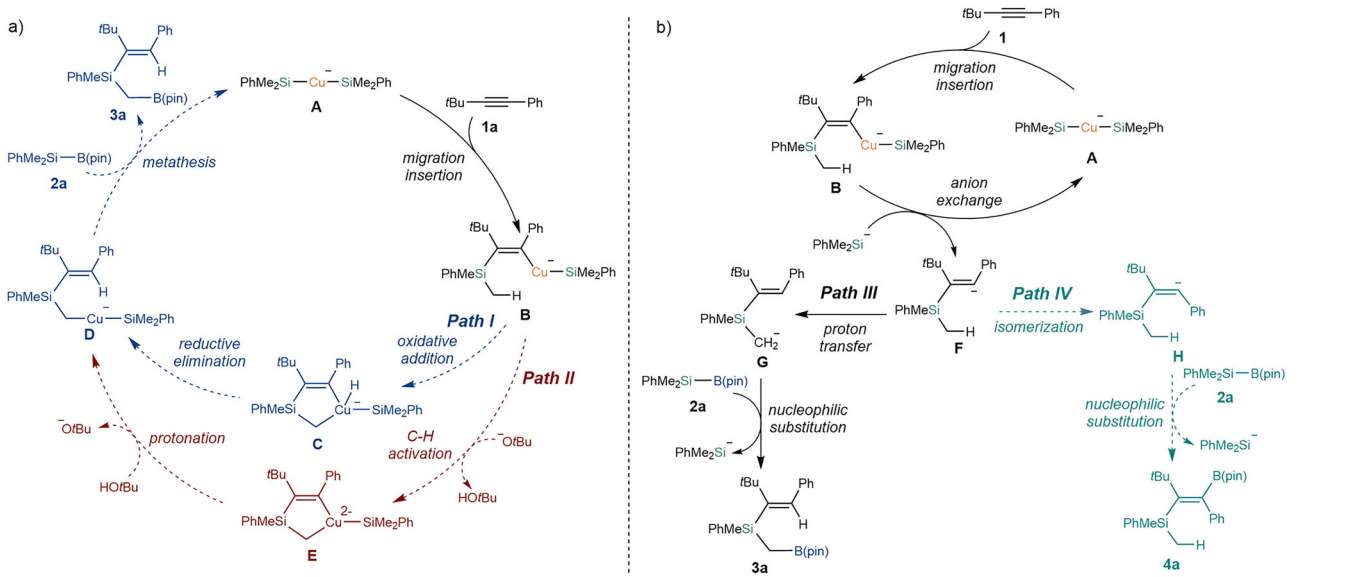

Scheme 2 | Proposed mechanism. **a** Proposed 1,4-copper migration mechanism. **b** Proposed metal non-migration mechanism.

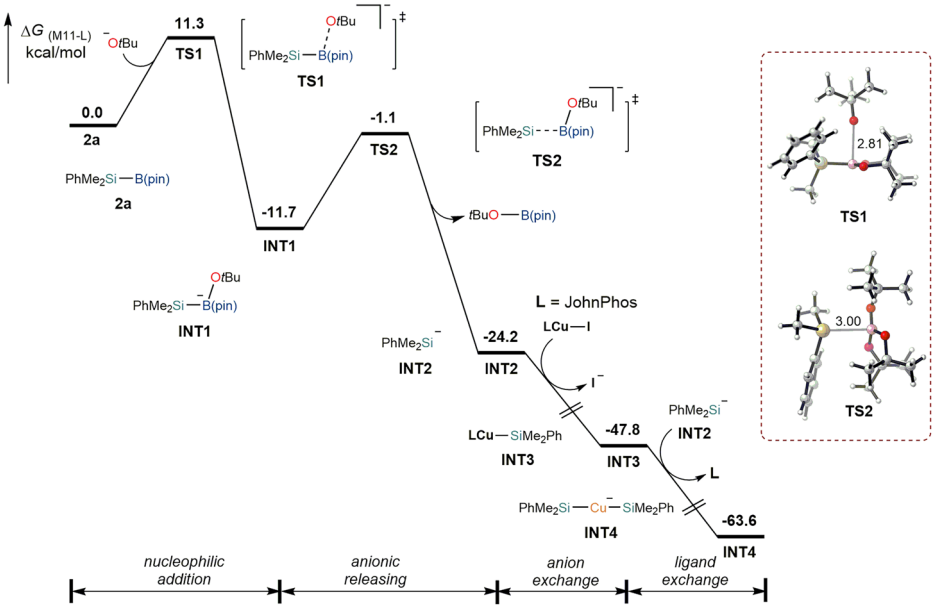

Fig. 1 | Calculated free energy profile. Free energy profile and selected structural information for the formation of the bis(phenyldimethylsilyl)cuprate active catalyst. Bond lengths are given in Å.

mixture. An anion exchange between **INT2** and the Cu(I)-I catalyst affords the silicon-Cu(I) intermediate **INT3**. Finally, a ligand exchange between **INT3** and **INT2** results in the formation of the anionic bis(phenyldimethylsilyl)cuprate active catalyst **INT4**, and this step is exoergic by 15.8 kcal/mol.

Figure 2 presents the calculated free energy profile for Path I. The computational results indicate that the migration and insertion of the internal alkyne substrate **1a** into the Cu(I)–Si bond in **INT4** follows a stepwise process, which includes coordination and migration insertion. Specifically, the coordination of alkyne substrate **1a** onto the Cu(I) center generates the Cu(I) intermediate, **INT5**. We calculated the oxidation state of the Cu center in **INT5** using Multiwfn program. The oxidation state of the Cu center in **INT5** was determined to be +1. The coordination step is followed by the migration insertion, which yields the anionic silane-substituted alkenyl-Cu(I) intermediate, **INT6**. The overall free energy barrier for the migration insertion transition state **TS4** is 27.8 kcal/mol, and the length of the forming C–Si bond is 2.58 Å. The subsequent 1,4-copper migration process involves oxidative addition and reductive elimination, which may occur via either a stepwise mechanism or a concerted pathway. During this process, the C(sp^3)–H bond undergoes oxidative addition by the Cu(I) center, resulting in the formation of the alkenyl- and alkyl-Cu(III) intermediate **INT7**. The free energy barrier for the oxidative addition transition state **TS5** is 33.2 kcal/mol. In **TS5**, the lengths of the forming C–Cu(I) bond and the breaking C–H bond are 2.08 and 1.73 Å, respectively. Then, **INT7** undergoes reductive elimination through transition state **TS6**, thereby generating the alkyl-Cu(I) intermediate **INT8** and completing the 1,4-copper migration process. Alternatively, the 1,4-copper migration may proceed via the concerted transition state **TS7**, which also results in the formation of **INT8**. In **TS7**, the lengths of the breaking C–H bond and the forming C–H bond are 1.57 and 1.33 Å, respectively. Notably, the free energy of **TS7** is 4.6 kcal/mol lower than that of **TS6**; however, the free energy barrier for **TS7** is high (33.6 kcal/mol), indicating that Path I is unfavorable. Subsequent metathesis between **INT8** and silylboronate **2a** occurs through a stepwise pathway. Nucleophilic addition of the carbanion

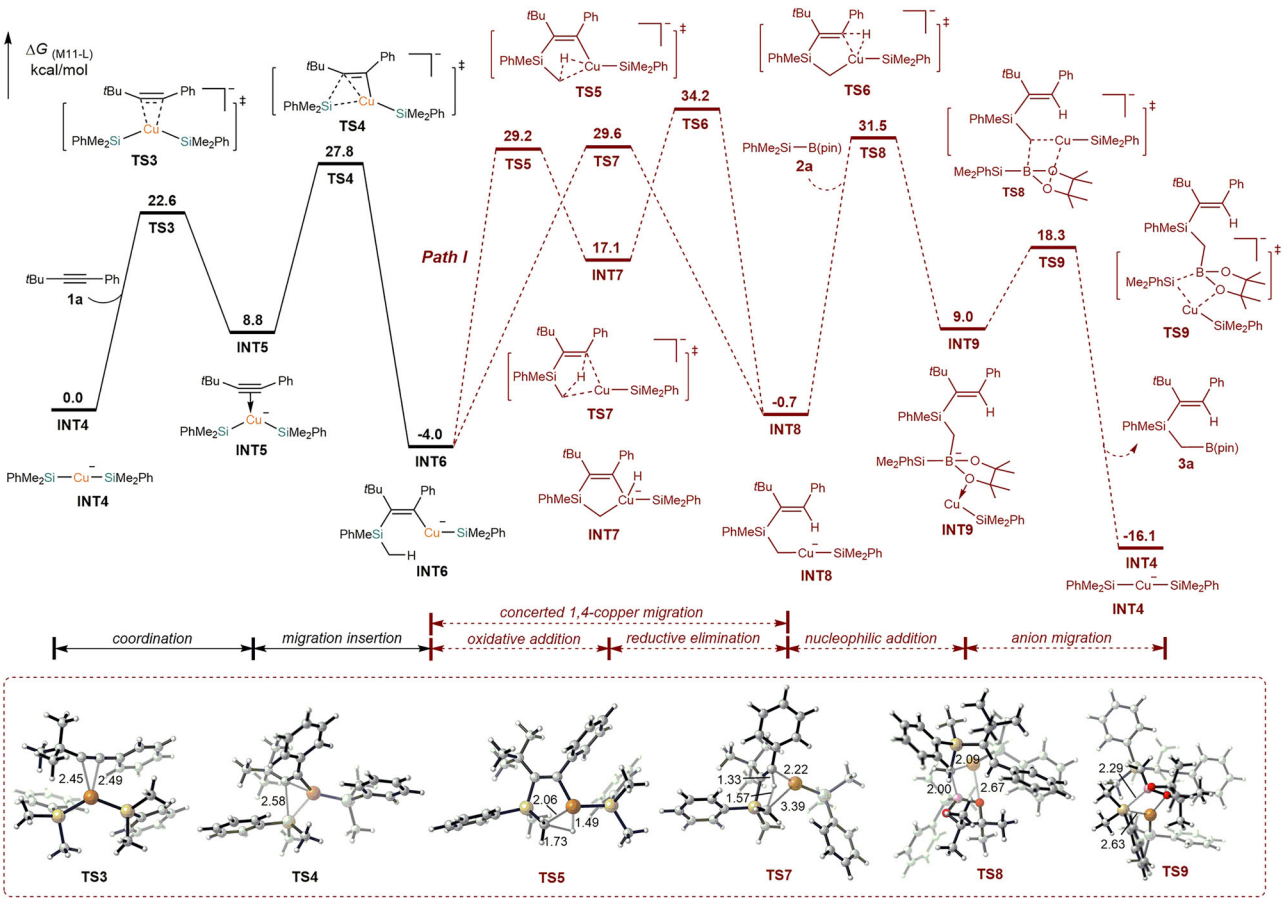

Fig. 2 | Calculated free energy profiles and selected structural information for Path I. Bond lengths are given in Å.

into silylboronate substrate **2a** generates the anionic boron intermediate **INT9**. The free energy barrier for the nucleophilic addition transition state **TS8** is 32.2 kcal/mol, and the lengths of the forming C–B bond and the breaking C–Cu bond measure 2.00 and 2.09 Å, respectively. Finally, the intramolecular migration of the silicon anion yields the alkenylsilylmethylboronate product **3a**, while regenerating the catalytically active species **INT4**, thus completing the catalytic cycle.

The calculated free energy profile for Path II is presented in Fig. 3. The alkenyl-Cu(I) anion intermediate **INT6** undergoes a CMD process via transition state **TS10**, using a *tert*-butoxide ion as a base, to form the alkenyl- and alkyl-Cu(I) intermediate **INT10**. The free energy barrier associated with **TS10** is 29.7 kcal/mol, and the lengths of the breaking C–H bond and the forming C–Cu bond are 1.96 and 2.36 Å, respectively. Subsequent protonation of the allyl C–Cu(I) bond occurs via transition state **TS11**, thereby yielding the alkyl-Cu(I) intermediate **INT8** and completing the 1,4-copper migration process. The overall activation barrier for this pathway is 31.2 kcal/mol, indicating that this 1,4-copper migration pathway is unfavorable. Additional calculations were employed to examine the use of silicon anions as a base to facilitate the 1,4-copper migration process. The free energy of the CMD transition state **TS10'** is 9.4 kcal/mol higher than that of **TS10**, and the free energy of the protonation transition state **TS11'** is 32.8 kcal/mol. These computational results suggest that Path II is also unfavorable.

As shown in Fig. 4a, the anion exchange reaction between the silicon anion and the alkenyl-Cu(I) anion intermediate **INT6** generates the alkenyl carbanion intermediate **INT11** and regenerates the catalytically active species **INT4**. The free energy barrier for the anion exchange transition state **TS12** is 19.4 kcal/mol. We used the silicon anion rather than the *tert*-butoxy anion because the former can be generated in situ in the presence of LiOtBu and methylsilyl boronic ester (Fig. 1). Moreover, we also consider the anion exchange between the *tert*-butoxide anion and the alkenyl-Cu(I) anion intermediate **INT6**. The free energy barrier for this anion exchange transition state **TS30** is 4.5 kcal/mol higher than that of **TS12** (Figure S4). Subsequent proton transfer from the methyl group to the alkenyl moiety occurs through transition state **TS13**, resulting in the formation of the alkyl carbanion intermediate **INT12**. The free energy barrier for the proton transfer transition state **TS13** is 21.6 kcal/mol, and the lengths of the forming C–H bond and the breaking C–H bond are 1.35 and 1.53 Å, respectively. Next, the nucleophilic addition of **INT12** to silylboronate **2a** produces the anionic boron intermediate **INT13**. Then, **INT13** releases an anionic silicon intermediate **INT2** via transition state **TS14**, yielding the alkenylsilylmethylboronate product **3a**. In **TS14**, the length of the breaking B–Si bond is 3.21 Å. These computational results show that the free energy of **TS12** is 14.2 kcal/mol lower than that of **TS7** and 11.8 kcal/mol lower than that of **TS11**, indicating that Path III is more favorable than Paths I and II.

Alternatively, in Path IV (Fig. 4b), the syn-to-anti isomerization of alkyl carbanion **INT11** produces the anti-alkyl carbanion intermediate **INT14**, with a low free energy barrier associated with the transition state **TS15** (2.2 kcal/mol). Subsequent nucleophilic addition of **INT14** into silylboronate **2a** affords the anionic boron intermediate **INT15**, and this process has a free energy barrier of 18.0 kcal/mol. In transition state **TS16**, the length of the forming C–B bond is 3.51 Å. Then, **INT15** releases the anionic silicon intermediate **INT2** via transition state **TS17**, yielding the by-product silylalkenylboronate **4a**; the length of the breaking B–Si bond in **TS17** is 3.46 Å. The free energy of **TS17** is 1.8 kcal/mol higher than that of **TS13**, while the free energy of **4a** exceeds that of **3a** by 5.7 kcal/mol. These kinetic and thermodynamic findings are consistent with the experimentally observed stereoselectivity ratio of 94:6, which favors product **3a** over **4a**. These findings are also consistent with those from deuterium substitution

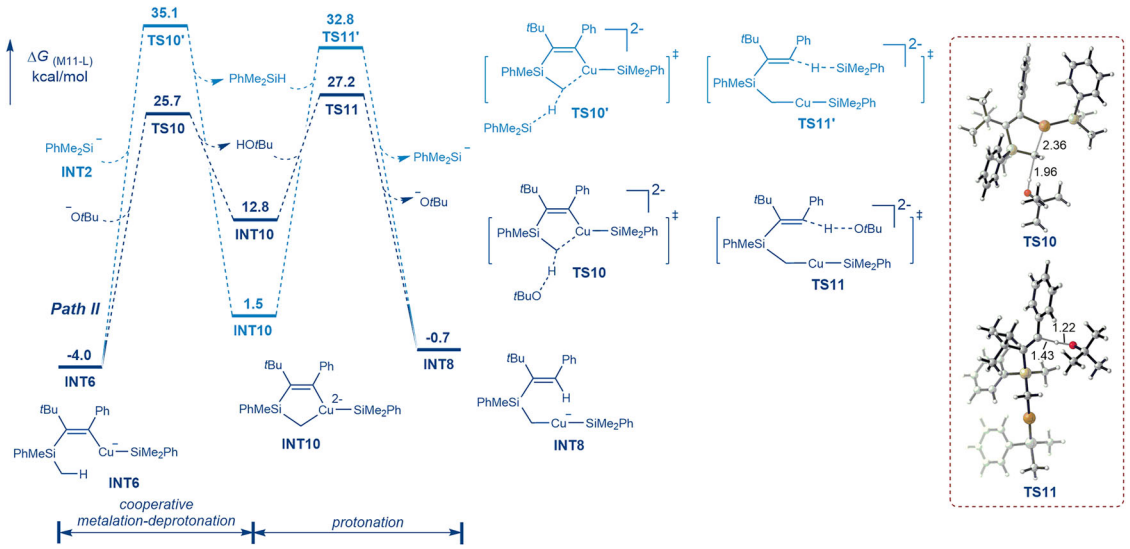

Fig. 3 | Free energy profile and selected structural information for Path II. Bond lengths are given in Å.

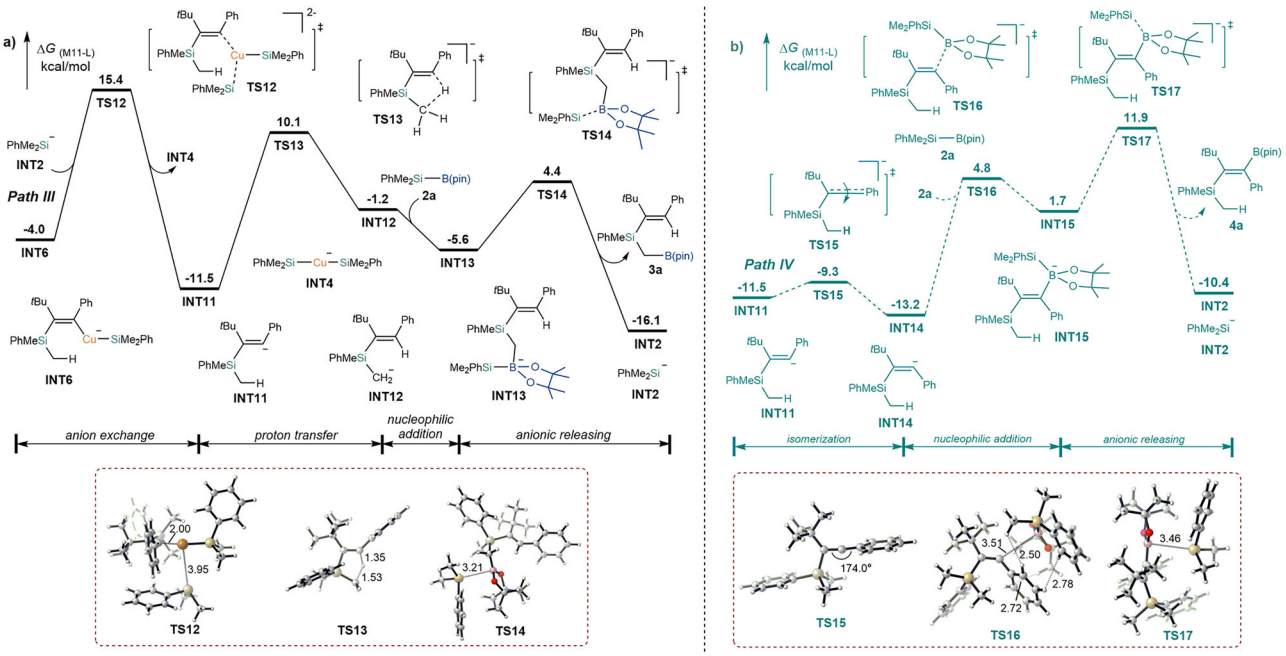

Fig. 4 | Free energy profile and selected structural information for Path III and Path IV. a Free energy profile for Path III. **b** Free energy profile for Path IV. Bond lengths are given in Å.

experiments[31]. When hydrogen was replaced with deuterium, the energy barrier for proton transfer increased, which reduced the yield of **3a**.

Our results indicated that the hydro(borylmethylsilyl)ation reaction pathway involved alkyne migration insertion, anion exchange, proton transfer, and nucleophilic substitution. Notably, the alkyne migration insertion step was identified as the rate-determining step in this reaction. This observation is consistent with kinetic experiments that demonstrate a first-order dependence on the concentration of the copper catalyst and a positive dependence (of approximately 0.5) on the initial concentration of the alkyne substrate[31].

Experimental results indicated that **3b** was preferentially formed over **4b** when alkyne **1b** containing an *ortho*-substituted aryl group was used in the reaction (Fig. 5). By contrast, **4c** was preferentially formed over **3c** when alkyne **1c** containing a less bulky isopropyl group was used in the reaction (Fig. 6)[31]. Thus, the substituent effects of the internal alkyne were evaluated using DFT calculations.

The computational results for the *ortho*-substituted aryl group substrate **1b** are presented in Fig. 5. As shown in Fig. 5a, proton transfer from the methyl group to the alkenyl moiety in the alkenyl carbanion intermediate **INT16** occurs via transition state **TS18**. This process forms the alkyl carbanion intermediate **INT17**, with a free energy barrier of 20.7 kcal/mol. In **TS18**, the lengths of the forming and breaking C–H bonds are 1.35 and 1.53 Å, respectively. Next, nucleophilic addition of **INT17** into silylboronate **2a** produces the anionic boron intermediate **INT18**. Subsequently, **INT18** releases the anionic silicon intermediate **INT2** via transition state **TS19**, yielding the alkenylsilylmethylboronate product **3b**; the length of the breaking B–Si bond in **TS19** is 3.27 Å.

As shown in Fig. 5b, In Path IV, the syn-to-anti isomerization of alkyl carbanion **INT16** yields the anti-alkyl carbanion **INT19**, with a low free

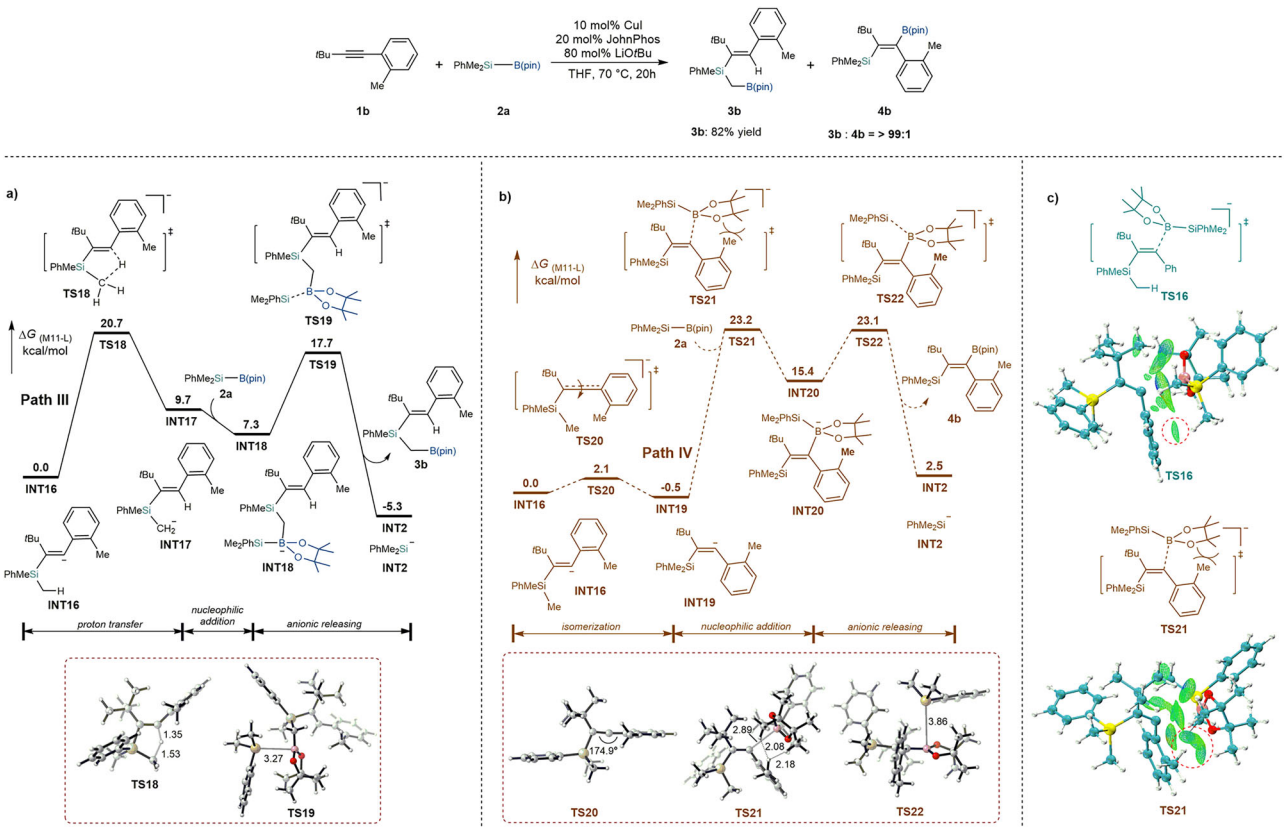

Fig. 5 | Free energy profile and selected structural information for Path III and Path IV using alkyne 1b with an *ortho*-substituted aryl group as the substrate. a Free energy profile for Path III. **b** Free energy profile for Path IV. **c** IGM analyses of **TS16** and **TS21**. Bond lengths are given in Å.

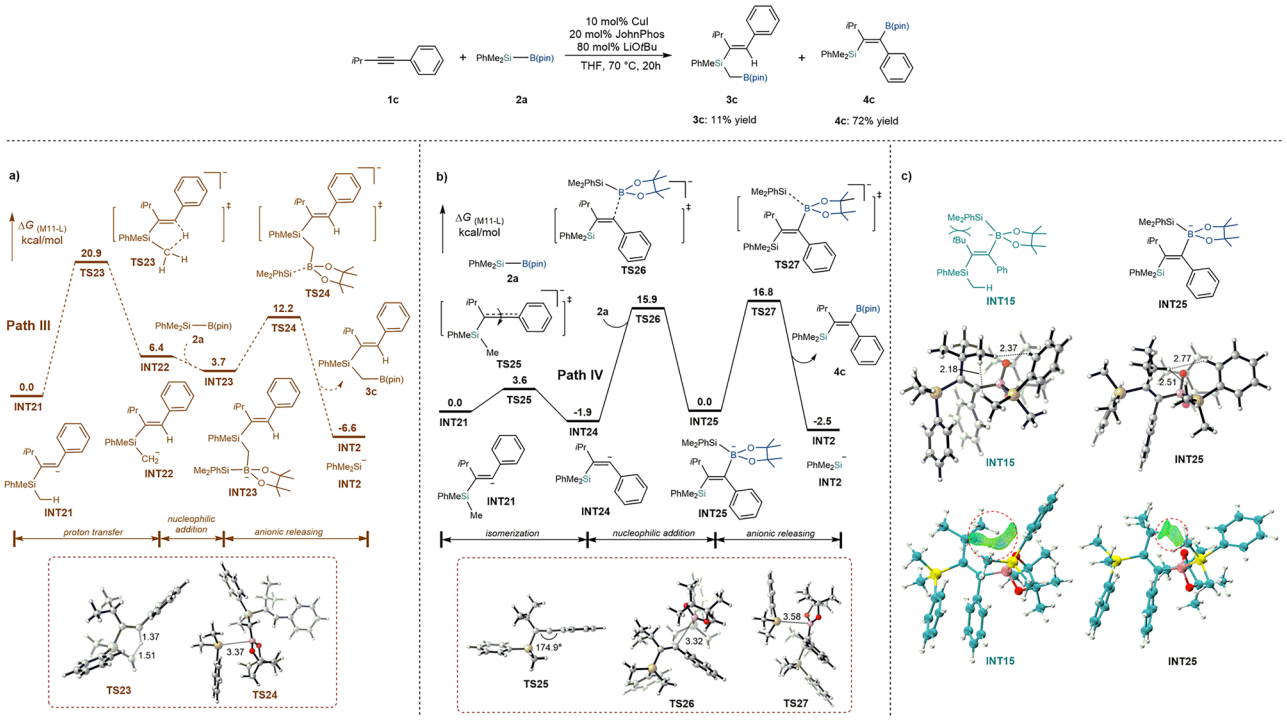

Fig. 6 | Free energy profile and selected structural information for Path III and Path IV using alkyne 1c, which contained a less bulky isopropyl group, as the substrate. a Free energy profile for Path III. **b** Free energy profile for Path IV. **c** IGM analyses of **INT15** and **INT25**. Bond lengths are given in Å.

energy barrier for transition state **TS20** (2.1 kcal/mol). The subsequent nucleophilic addition of **INT19** into silylboronate **2a** forms the anionic boron intermediate **INT20**. This step has a free energy barrier of 23.7 kcal/mol, and the forming C–B bond in transition state **TS21** is 2.89 Å. Then, **INT20** releases the anionic silicon intermediate **INT2** via transition state **TS22**, producing the by-product silylalkenylboronate **4b**; the length of the breaking B–Si bond length in **TS22** is 3.86 Å. Notably, the free energy of **TS21** is 2.5 kcal/mol higher than that of **TS18**, whereas the free energy of **4b** is 7.8 kcal/mol greater than that of **3b**. These kinetic and thermodynamic results are consistent with the experimentally observed stereoselectivity, with a ratio of 99:1 in favor of product **3b** over **4b**.

Independent gradient model (IGM) calculations were performed for **TS16** and **TS21** to explore the origin of the high stereoselectivity for **3b** over **4b** when alkyne **1** has an *ortho*-substituted aryl group (Fig. 5c). In **TS16**, the closest H···H distance between the phenyl group and silylboronate **2a** is 2.50 Å (Fig. 4b), while in **TS21** the closest H···H distance between the *ortho*-substituted phenyl group and silylboronate **2a** is 2.08 Å (Fig. 5b). The results indicated that the electrostatic repulsion between the *ortho*-substituted aryl group and silylboronate **2a** in **TS21** is stronger than that between the phenyl group and silylboronate **2a** in **TS16**, which leads to the high stereoselectivity.

The computational results for the less bulky isopropyl group substrate **1c** are presented in Fig. 6. Proton transfer from the methyl group to the alkenyl moiety in the alkenyl carbanion intermediate **INT21** occurs through transition state **TS23** (Fig. 6a). This transfer gives the alkyl carbanion intermediate **INT22**, which has a free energy barrier of 20.9 kcal/mol. In transition state **TS23**, the lengths of the C–H bonds that formed and broke were 1.37 Å and 1.51 Å, respectively. Next, nucleophilic addition of **INT22** to silylboronate **2a** generates the anionic boron intermediate **INT23**. Subsequently, **INT23** transforms into the anionic silicon intermediate **INT2** via transition state **TS24**, which results in the formation of the alkenylsilylmethylboronate product **3c**. The length of the B–Si bond that breaks in **TS24** is 3.37 Å.

The syn-to-anti isomerization of alkyl carbanion **INT21** results in formation of the anti-alkyl carbanion **INT24**, with a low free energy barrier of 3.6 kcal/mol for transition state **TS25** (Fig. 6b). Subsequent nucleophilic addition of **INT24** to silylboronate **2a** generates the anionic boron intermediate **INT25**, with a free energy barrier of 17.8 kcal/mol. In transition state **TS26**, the length of the C–B bond that forms is 3.32 Å. Next, **INT25** transitions to the anionic silicon intermediate **INT2** via transition state **TS27**, which produces the silylalkenylboronate **4c**. The length of the B–Si bond that breaks in **TS27** is 3.58 Å. Notably, the free energy of **TS27** is 4.1 kcal/mol lower than that of **TS23**, but the free energy of **4c** is 4.1 kcal/mol higher than that of **3c**. These kinetic and thermodynamic findings are consistent with the experimentally observed stereoselectivity of products **4c** and **3c**.

A comparison of the results from Figs. 4b, 6b revealed that the lower energy of **TS26** could be attributed to the fact that the energy of intermediate **INT25** was lower than that of **INT15**. IGM calculations were conducted for **INT15** and **INT25** to investigate the origin of stereoselectivity inversion when the alkyne **1c**, which contained a less bulky isopropyl group, was used as the substrate (Fig. 6c). In addition, the closest H···H distance between the *tert*-butyl group and dimethylphenylsilyl moiety in silylboronate **2a** is 2.18 Å in **INT15**, while in **INT25** the closest H···H distance between the isopropyl group and dimethylphenylsilyl group in silylboronate **2a** is 2.51 Å. The calculated results indicated that electrostatic repulsion between the *tert*-butyl group and the dimethylphenylsilyl moiety in silylboronate **2** in **INT15** was stronger than that between the isopropyl group and the dimethylphenylsilyl group in silylboronate **2** in **INT25**. This heightened repulsion contributed to the higher energy of **INT15** compared with **INT25**.

Conclusion

In this study, DFT calculations were performed to explore the mechanism governing a Cu-catalyzed formal hydro(borylmethylsilyl)ation reaction. Specifically, the feasibility of 1,4-copper migration was evaluated within an established theoretical framework. The results indicated that the 1,4-copper migration pathway is kinetically unfavorable, regardless of whether it proceeds through an oxidative addition and reductive elimination pathway or via a cooperative metalation-deprotonation and protonation mechanism. Theoretical calculations revealed that the hydro(borylmethylsilyl)ation reaction involves alkyne migration insertion, anion exchange, proton transfer, and nucleophilic substitution. The alkyne migration insertion step was identified as the rate-determining step in this reaction. The stereoselectivity of products was dictated by the energy difference between the proton transfer transition state and the anionic releasing transition state following syn-to-anti isomerization. Additionally, the effect of substituents on the internal alkyne was assessed using DFT calculations. The results demonstrated that steric hindrance between the *ortho*-methyl group and the silylboronate substrate enhanced the stereoselectivity. By contrast, lower steric hindrance between the isopropyl group and the dimethylphenylsilyl moiety resulted in stereoselectivity inversion. Overall, the findings presented in this report advance the understanding of Cu-catalyzed migration coupling reactions and provide a theoretical framework for guiding future experimental investigations.

Data availability

The data supporting the findings of this study are included in the paper or the Supplementary Information and are also available upon request from the corresponding author. The geometries of all optimized compounds and transition states have been deposited in the Supplementary Data.

Received: 11 July 2025; Accepted: 24 November 2025;
Published online: 09 December 2025

References

1. Li, Y.-Q., Wu, D., Cheng, H.-G. & Yin, G.-Y. Difunctionalization of Alkenes Involving Metal Migration. *Angew. Chem. Int. Ed.* **59**, 7990–8003 (2016).
2. Dong, X., Wang, H., Liu, H. & Wang, F. Recent advances in transition metal migration involving reactions. *Org. Chem. Front.* **7**, 3530–3556 (2020).
3. Rahim, A., Feng, J. & Gu, Z. 1,4-Migration of Transition Metals in Organic Synthesis. *Chin. J. Chem.* **37**, 929–945 (2019).
4. Shi, F., Larock, R. C., Yu, J. Q. & Shi, Z. Remote C−H Activation via Through-Space Pallaium and Rhodium Migrations. *Top. Curr. Chem.* **292**, 123–164 (2010).
5. Liu, S., Zhang, D., Zhang, X., Cheng, Y. & Deng, H. Investigation of the activation mode of vinylarene in Giri's Ni-catalyzed vinylarene intermolecular 1,2-alkylarylation cross-coupling: a theoretical study. *Org. Chem. Front.* **10**, 4359–4367 (2023).
6. Li, W.-C. et al. Synthesis of benzoheterocycles by palladium-catalyzed migratory cyclization through an unexpected reaction cascade. *Nat. Commun.* **16**, 3367 (2025).
7. Tsitopoulou, M., Clemenceau, A., Thesmar, P. & Baudoin, O. 1,4-Pd Migration-Enabled Synthesis of Fused 4 Membered Rings. *J. Am. Chem. Soc.* **146**, 18811–18816 (2024).
8. Chen, Y.-W., Liu, Y., Lu, H.-Y., Lin, G.-Q. & He, Z.-T. Palladium-catalyzed regio- and enantioselective migratory allylic C(sp^3)-H functionalization. *Nat. Commun.* **12**, 5626 (2021).
9. Tsuda, T., Kawakami, Y., Choi, S.-M. & Shintani, R. Palladium-Catalyzed Synthesis of Benzophnanthrosilines by C−H/C−H Coupling through 1,4-Palladium Migration/Alkene Stereoisomerization. *Angew. Chem., Int. Ed.* **59**, 8057–8061 (2020).
10. Rocaboy, R., Anastasiou, I. & Baudoin, O. Redox-Neutral Coupling between Two C(sp^3)−H Bonds Enabled by 1,4-Palladium Shift for the Synthesis of Fused Heterocycles. *Angew. Chem., Int. Ed.* **58**, 14625–14628 (2019).
11. Hikida, N., Yoshimi, Y. & Suzuki, H. Amide-Directed Rhodium-Catalyzed Chain-Walking Hydrothiolation of Internal Alkenes. *Org. Lett.* **26**, 2500–2504 (2024).

12. Guo, C.-X., Xing, D.-H., Jiang, H.-F. & Huang, L.-B. Redox-neutral ipso/ortho alkenylcyanation of (hetero)arylboronic acid enabled by 1,4-rhodium migration and fragmentation. *Sci. China Chem.* **66**, 2283–2291 (2023).
13. Groves, A. et al. Catalytic enantioselective arylative cyclizations of alkynyl 1,3-diketones by 1,4-rhodium(I) migration. *Chem. Sci.* **11**, 2759–2764 (2020).
14. Zhang, S.-S. et al. Asymmetric Alkenylation of Enones and Imines Enabled by A Highly Efficient Aryl to Vinyl 1,4-Rhodium Migration. *Angew. Chem., Int. Ed.* **58**, 3387–3391 (2019).
15. Kimura, N., Kochi, T. & Kakiuchi, F. Iron-Catalyzed Ortho-Selective C−H Alkylation of Aromatic Ketones with N-Alkenylindoles and Partial Indolylation via 1,4-Iron Migration. *Asian J. Org. Chem.* **8**, 1115–1117 (2019).
16. Mo, J., Müller, T., Oliveira, J. C. A. & Ackermann, L. 1,4-Iron Migration for Expedient Allene Annulations through Iron-Catalyzed C−H/N−H/C−O/C−H Functionalizations. *Angew. Chem., Int. Ed.* **57**, 7719–7723 (2018).
17. Chen, J. et al. Cobalt-Catalyzed Asymmetric Migratory Nozaki−Hiyama−Kishi Coupling. *J. Am. Chem. Soc.* **146**, 26223–26232 (2024).
18. Park, J. Cobalt-catalyzed alkyne hydrosilylation as a new frontier to selectively access silyl-hydrocarbons. *Chem. Commun.* **58**, 491–504 (2022).
19. Sahoo, M. K., Kim, D., Chang, S. & Park, J.-W. Regioselective Access to α-Vinylsilanes and α-Vinylgermanes by Cobalt-Catalyzed Migratory Hydrofunctionalization of 2-Alkynes. *ACS Catal.* **11**, 12777–12784 (2021).
20. Yan, J. & Yoshikai, N. Cobalt-Catalyzed Arylative Cyclization of Acetylenic Esters and Ketones with Arylzinc Reagents through 1,4-Cobalt Migration. *ACS Catal.* **6**, 3738–3742 (2016).
21. Tan, B.-H. & Yoshikai, N. Cobalt-Catalyzed Addition of Arylzinc Reagents to Norbornene Derivatives through 1,4-Cobalt Migration. *Org. Lett.* **16**, 3392–3395 (2014).
22. Tan, B.-H., Dong, J. & Yoshikai, N. Cobalt-Catalyzed Addition of Arylzinc Reagents to Alkynes to Form ortho-Alkenylarylzinc Species through 1,4-Cobalt Migration. *Angew. Chem., Int. Ed.* **51**, 9610–9614 (2012).
23. Ding, L. et al. Stereoselective Vinylic C−H Addition via Metallaphotoredox Migration. *Angew. Chem. Int. Ed.* **64**, e202413557 (2025).
24. Lee, D., Fujii, I. & Shintani, R. Nickel-Catalyzed Synthesis of Silaindanes via Sequential C−H Activating 1,5-Nickel Migration and C−Si Activating 1,4-Nickel Migration. *ACS Catal.* **15**, 907–916 (2025).
25. Zhang, H., Rodrigalvarez, J. & Martin, R. C(sp^2)−H Hydroxylation via Catalytic 1,4-Ni Migration with N_2O. *J. Am. Chem. Soc.* **145**, 17564–17569 (2023).
26. Yang, J., Gui, Z., He, Y. & Zhu, S. Functionalization of Olefinic C−H Bonds by an Aryl-to-Vinyl 1,4-Nickel Migration/Reductive Coupling Sequence. *Angew. Chem., Int. Ed.* **62**, e202304713 (2023).
27. Wang, C.-T. et al. Aryl-to-Vinyl 1,4-Nickel Migration/Reductive Cross-Coupling Reaction Applied to the Stereoselective Synthesis of Multisubstituted Olefins. *Angew. Chem., Int. Ed.* **62**, e202304447 (2023).
28. Li, Y. & Yin, G. Nickel Chain-Walking Catalysis: A Journey to Migratory Carboboration of Alkenes. *Acc. Chem. Res.* **56**, 3246–3259 (2023).
29. He, Y. et al. Nickel-Catalyzed ipso/ortho Difunctionalization of Aryl Bromides with Alkynes and Alkyl Bromides via a Vinyl-to-Aryl 1,4-Hydride Shift. *J. Am. Chem. Soc.* **143**, 20064–20070 (2021).
30. Borjesson, M. et al. Remote sp^2 C−H Carboxylation via Catalytic 1,4-Ni Migration with CO_2. *J. Am. Chem. Soc.* **142**, 16234–16239 (2020).
31. Moniwa, H., Yamanaka, M. & Shintani, R. Copper-Catalyzed Regio- and Stereoselective Formal Hydro(borylmethylsilyl)ation of Internal Alkynes via Alkenyl-to-Alkyl 1,4-Copper Migration. *J. Am. Chem. Soc.* **145**, 23470–23477 (2023).
32. Zhang, S.-S. et al. Asymmetric Alkenylation of Enones and Imines Enabled by AHighly Efficient Aryl to Vinyl 1,4-Rhodium Migration. *Angew. Chem. Int. Ed.* **58**, 3387–3391 (2019).
33. Liu, N. et al. Rhodium-Catalyzed Expeditious Synthesis of Indenes from Propargyl Alcohols and Organoboronic Acids by Selective 1,4 Rhodium Migration over β Oxygen Elimination. *ACS Catal.* **9**, 6857–6863 (2019).
34. Xu, B., Ji, D.-T., Zhang, Z.-M. & Zhang, J.-L. Remote C−H Bond Activation via Enantioselective Carbopalladation and 1,4-Pd Migration Cascade Process. *Adv. Sci.* **11**, 2406443 (2024).
35. Wang, Q.-N. et al. Highly Regioselective C−H Alkylation of Alkenes Through an Aryl to Vinyl 1,4-Palladium Migration/C−C Cleavage Cascade. *ACS Catal.* **9**, 11669–11675 (2019).
36. Li, W.-F., Boon, J.-K. & Zhao, Y. Nickel-catalyzed difunctionalization of allyl moieties using organoboronic acids and halides with divergent regioselectivities. *Chem. Sci.* **9**, 600–607 (2018).
37. Basnet, P. et al. Ni-Catalyzed Regioselective β,δ-Diarylation of Unactivated Olefins in Ketimines via Ligand-Enabled Contraction of Transient Nickellacycles: Rapid Access to Remotely Diarylated Ketones. *J. Am. Chem. Soc.* **140**, 7782–7786 (2018).
38. Jeon, J. et al. Site-Selective 1,1-Difunctionalization of Unactivated Alkenes Enabled by Cationic Palladium Catalysis. *J. Am. Chem. Soc.* **141**, 10048–10059 (2019).
39. Zhang, Z., Chena, P. & Liu, G. Copper-catalyzed radical relay in C(sp^3)–H functionalization. *Chem. Soc. Rev.* **51**, 1640–1658 (2022).
40. Yang, Y. et al. Recent Advances in Copper Promoted Inert C(sp^3)−H Functionalization. *ACS Catal.* **11**, 967–984 (2021).
41. Kim, H. Y. & Oh, K. Recent advances in the copper-catalyzed aerobic Csp^3−H oxidation strategy. *Org. Biomol. Chem.* **19**, 3569–3583 (2021).
42. García-Viada, A., Carretero, J. C., Adrio, J. & Rodríguez, N. Insights into the mechanism of 3d transitionmetal-catalyzed directed C(sp^3)−H bond functionalization reactions. *Chem. Soc. Rev.* **54**, 4353–4390 (2025).
43. Liu, J., Chen, G. & Tan, Z. Copper-Catalyzed or -Mediated C−H Bond Functionalizations Assisted by Bidentate Directing Groups. *Adv. Synth. Catal.* **358**, 1174–1194 (2016).
44. Blythe, I. M. et al. Characterization and Reactivity of Copper(II) and Copper(III) σ-Aryl Intermediates in Aminoquinoline-Directed C−H Functionalization. *J. Am. Chem. Soc.* **145**, 18253–18259 (2023).
45. Tan, G. et al. Copper- or Nickel-Enabled Oxidative Cross-Coupling of Unreactive C(sp^3)−H Bonds with Azole C(sp^2)−H Bonds: Rapid Access to *β*-Azolyl Propanoic Acid Derivatives. *Org. Lett.* **19**, 4830–4833 (2017).
46. Watanabe, K., Nagao, K. & Ohmiya, H. Deoxygenative Geminal Silylboration of Amides Using Silylboronates: Synthesis and Use of α-Boryl-α-Silylalkylamines. *Angew. Chem. Int. Ed.* **63**, e202411990 (2024).
47. Jeong, E., Heo, J., Jin, S., Kim, D. & Chang, S. KO*t*Bu-Catalyzed 1,2-Silaboration of N-Heteroarenes to Access 2-Silylheterocycles: A Cooperative Model for the Regioselectivity. *ACS Catal.* **12**, 4898–4905 (2022).
48. Gao, P. et al. Transition-Metal-Free Defluorosilylation of Fluoroalkenes with Silylboronates. *Chin. J. Chem.* **37**, 1009–1014 (2019).
49. Shintani, R., Fujie, R., Takeda, M. & Nozaki, K. Silylative Cyclopropanation of Allyl Phosphates with Silylboronates. *Angew. Chem. Int. Ed.* **53**, 6546–6549 (2014).
50. Li, H. et al. Formal Carbon Insertion of N-Tosylhydrazone into B−B and B−Si Bonds: *gem*-Diborylation and *gem*-Silylborylation of sp^3 Carbon. *Org. Lett.* **16**, 448–451 (2013).
51. Wang, L. et al. C−O Functionalization of α-Oxyboronates: A Deoxygenative *gem*-Diborylation and *gem*-Silylborylation of Aldehydes and Ketones. *J. Am. Chem. Soc.* **139**, 5257–5264 (2017).

52. Frisch, M. J. et al. Gaussian 16, Revision A.03, Gaussian, Inc., Wallingford, CT, 2016, The full author list is given in the ESI.
53. Becke, A. D. Density-functional thermochemistry. III. The role of exact exchange. *J. Chem. Phys.* **98**, 5648–5652 (1993).
54. Lee, C., Yang, W. & Parr, R. G. Development of the Colle-Salvetticorrelation-energy formula into a functional of the electron density. *Phys. Rev. B: Condens. Matter Mater. Phys.* **37**, 785–789 (1988).
55. Schmider, H. L. & Becke, A. D. Optimized density functionals from the extended G2 test set. *J. Chem. Phys.* **108**, 9624–9631 (1998).
56. Becke, A. D. et al. A density-functional model of the dispersion interaction. *J. Chem. Phys.* **123**, 154101 (2005).
57. Grimme, S. et al. Effect of the damping function in dispersion corrected density functional theory. *J. Comput. Chem.* **32**, 1456–1465 (2011).
58. Grimme, S. et al. A consistent and accurate ab initio parametrization of density functional dispersion correction (DFT-D) for the 94 elements H-Pu. *J. Chem. Phys.* **132**, 154104 (2010).
59. Cossi, M., Barone, V., Cammi, R. & Tomasi, J. Ab initio study of solvated molecules: a new implementation of the polarizable continuum model. *Chem. Phys. Lett.* **255**, 327–335 (1996).
60. Peverati, R. & Truhlar, D. G. Improving the Accuracy of Hybrid Meta-GGA Density Functionals by Range Separation. *J. Phys. Chem. Lett.* **2**, 2810–2817 (2011).
61. Andrae, D., Häußermann, U., Dolg, M., Stoll, H. & Preuß, H. Energy-adjustedab initio pseudopotentials for the second and third row transition elements. *Theor. Chim. Acta* **77**, 123–141 (1990).
62. Weigend, F. & Ahlrichs, R. Balanced basis sets of split valence, triple zeta valence and quadruple zeta valence quality for H to Rn: Design and assessment of accuracy. *Phys. Chem. Chem. Phys.* **7**, 3297–3305 (2005).
63. Legault, C. Y. CYLView, version 1.0b; Université de Sherbrooke: Canada, http://www.cylview.org. (Date of access:1/10/2017) (2009).
64. Lu, T. et al. Multiwfn: A multifunctional wavefunction 901 analyzer. *J. Comput. Chem.* **33**, 580–592 (2012).
65. Johnson, E. R. et al. Revealing Noncovalent Interactions. *J. Am. Chem. Soc.* **132**, 6498–6506 (2010).
66. Humphrey, W. et al. VMD: visual molecular dynamics. *J. Mol. Graph.* **14**, 33–38 (1996).
67. Fang, D.-C. THERMO; Beijing Normal University, Beijing, People's Republic of China (2013).

Acknowledgements

This work was supported by the National Natural Science Foundation of China (No. 22303010 and 22271034). We are thankful to the Science and Technology Research Program of Chongqing Municipal Education Commission for financial support (No. KJQN202301354). This project was also funded by the Project of Financial support of Chongqing University of Arts and Sciences (No. P2021HH04).

Author contributions

S. Liu conceived and designed the project and designed the computational studies. W. Chen, X. Long, D. Zhang, and J. Chen performed the DFT calculations. S. Liu and W. Chen prepared the manuscript. Z. Zhu and H. Wei prepared the ESI.

Competing interests

The authors declare no competing interests.

Additional information

Supplementary information The online version contains supplementary material available at https://doi.org/10.1038/s42004-025-01829-z.

Correspondence and requests for materials should be addressed to Song Liu or Wei Chen.

Peer review information *Communications Chemistry* thanks the anonymous reviewers for their contribution to the peer review of this work.